Eur. Phys. J. A **10**, 207–215 (2001)

THE EUROPEAN PHYSICAL JOURNAL A

Low-energy Compton scattering and the polarizabilities of the proton

V. Olmos de León[1,a], F. Wissmann[2,b,c], P. Achenbach[3,d], J. Ahrens[1], H.-J. Arends[1], R. Beck[1], P.D. Harty[4], V. Hejny[3,e], P. Jennewein[1], M. Kotulla[3], B. Krusche[3,f], V. Kuhr[2], R. Leukel[1], J.C. McGeorge[4], V. Metag[3], R. Novotny[3], A. Polonski[5], F. Rambo[2], A. Schmidt[1], M. Schumacher[2], U. Siodlaczek[6], H. Ströher[3,g], A. Thomas[1], J. Weiß[3], and M. Wolf[3]

[1] Institut für Kernphysik, Universität Mainz, D-55099 Mainz, Germany
[2] II. Physikalisches Institut, Universität Göttingen, D-37073 Göttingen, Germany
[3] II. Physikalisches Institut, Universität Giessen, D-35392 Giessen, Germany
[4] Department of Physics and Astronomy, University of Glasgow, Glasgow G12 8QQ, UK
[5] INR, Russian Academy of Sciences, Moscow, Russia
[6] Physikalisches Institut, Universität Tübingen, D-72076 Tübingen, Germany

Received: 9 January 2001 / Revised version: 8 February 2001
Communicated by M. Garçon

Abstract. Differential cross-sections for Compton scattering from the proton have been measured at the MAMI tagged photon facility using the TAPS setup. The data cover an angular range of $\theta_\gamma^{\rm lab} = 59^\circ$–$155^\circ$ and photon energies ranging from 55 MeV to 165 MeV. Our results are in good agreement with those from previous experiments, but yield higher precision. Using dispersion relations the proton polarizabilities have been determined to be $\bar{\alpha} = [11.9 \pm 0.5_{\rm stat.} \mp 1.3_{\rm syst.} \pm 0.3_{\rm mod.}] \cdot 10^{-4}$ fm^3 and $\bar{\beta} = [1.2 \pm 0.7_{\rm stat.} \pm 0.3_{\rm syst.} \pm 0.4_{\rm mod.})] \cdot 10^{-4}$ fm^3. These results confirm the Baldin sum rule which was re-evaluated to be $\bar{\alpha} + \bar{\beta} = [13.8 \pm 0.4] \cdot 10^{-4}$ fm^3. We can also conclude that there is no significant additional asymptotic contribution to the backward spin polarizability γ_π beyond the t-channel π^0-exchange.

PACS. 11.55.Fv Dispersion relation – 13.60.Fz Elastic and Compton scattering – 14.20.Dh Proton and neutrons – 25.20.Dc Photon absorption and scattering

1 Introduction

At incident photon energies far below the π-production threshold, *i.e.* $\omega \to 0$, photon scattering from the proton is described completely by the proton's static properties mass and charge, which corresponds to the scattering of an electromagnetic wave from a point particle with mass m and charge e (Thomson scattering). This scattering process is described by the scattering amplitude

$$f_{\rm Th} = -\frac{e^2}{m}\,\epsilon'\epsilon\ . \tag{1}$$

Here, ϵ' and ϵ are the polarization vectors of the incident and the scattered photon.

With increasing photon energy additional terms arise due to the magnetic moment μ. For the proton these terms were calculated by Low [1], Gell-Mann and Goldberger [2], and Klein [3] in their fundamental articles. They give an expression for the expansion of the scattering amplitude up to terms linear in the photon energy ω.

Petrun'kin [4,5] developed the complete scattering amplitude in a low-energy expansion up to order ω^2,

[a] Part of the *doctoral* thesis.
[b] Part of the *habilitation* thesis.
[c] *Present address*: Physikalisch-Technische Bundesanstalt, Bundesallee 100, D-38116 Braunschweig, Germany.
e-mail: `fwissma@gwdg.de`
[d] *Present address*: Institut für Kernphysik, Universität Mainz, D-55099 Mainz, Germany.
[e] *Present address*: Forschungszentrum Jülich, Institut für Kernphysik, D-52425 Jülich, Germany.
[f] *Present address*: Department of Physics and Astronomy, University of Basel, CH-4056 Basel, Switzerland.
[g] *Present address*: Forschungszentrum Jülich, Institut für Kernphysik, D-52425 Jülich, Germany.

$$
\begin{aligned}
f_{\rm Pet} = & -\frac{e^2}{m}\epsilon'\epsilon + i\,(\omega'+\omega)\,\frac{e^2}{4m^2}\,(1+2\kappa)\,\sigma\,(\epsilon'\times\epsilon) \\
& -i(\omega'+\omega)\frac{e^2}{4m^2}\,(1+\kappa)^2\,\sigma[(\mathbf{n}'\times\epsilon')\times(\mathbf{n}\times\epsilon)] \\
& +i\frac{e^2}{2m^2}\,(1+\kappa)\,[\omega'\,(\mathbf{n}'\epsilon)\,\sigma\,(\mathbf{n}'\times\epsilon') \\
& \qquad -\omega\,(\mathbf{n}\epsilon')\sigma(\mathbf{n}\times\epsilon)] \\
& +\omega'\omega\frac{e^2}{4m^3}\left(2\kappa+\kappa^2\right)\epsilon'\epsilon \\
& -\omega'\omega\frac{e^2}{4m^3}\,(1+\kappa)^2\,(\mathbf{n}'\times\epsilon')\,(\mathbf{n}\times\epsilon)\,(\mathbf{n}'\mathbf{n}) \\
& +\omega'\omega\frac{e^2}{4m^3}\,(\mathbf{n}'\times\epsilon')\,(\mathbf{n}\times\epsilon) \\
& +\omega'\omega[\bar{\alpha}\epsilon'\epsilon+\bar{\beta}\,(\mathbf{n}'\times\epsilon')\,(\mathbf{n}\times\epsilon)]\,, \qquad (2)
\end{aligned}
$$

with the anomalous magnetic moment κ of the proton, the electric and magnetic polarizabilities $\bar{\alpha}$ and $\bar{\beta}$, respectively, and the directions $\mathbf{n}$, $\mathbf{n}'$ and energies ω, ω' of the incident and the scattered photon, respectively, with $\mathbf{n}'\mathbf{n} = \cos\theta_\gamma$, where θ_γ is the photon scattering angle in the lab-system. The first term on the r.h.s of eq. (2) is the Thomson-amplitude $f_{\rm Th}$ given in eq. (1). The following six terms describe the scattering due to the magnetic moment. This part had been evaluated by Powell [6] already in 1949 and was given in an appendix of his article about bremsstrahlung. Up to here the proton is assumed to be a point-like particle. The last term on the r.h.s of eq. (2) is related to the internal structure of the proton and is expressed in terms of the electromagnetic polarizabilities $\bar{\alpha}$ and $\bar{\beta}$ [1].

Calculating the differential cross-section by squaring the amplitude, gives rise to ω^2-terms i) due to the terms linear in ω or ω', and ii) due to the interference of the Thomson amplitude $f_{\rm Th}$ and the terms proportional to $\omega\omega'$. Squaring the amplitude (2), averaging over the incident photon polarizations and proton spin states and summing over the final ones yields the differential cross-section for scattering of unpolarized photons from unpolarized protons [4,5]:

$$
\begin{aligned}
\left(\frac{{\rm d}\sigma}{{\rm d}\Omega}\right) &= \left(\frac{{\rm d}\sigma}{{\rm d}\Omega}\right)_{\rm Point} \\
&-\omega\omega'\left(\frac{\omega'}{\omega}\right)^2\frac{e^2}{m}\left[\frac{\bar{\alpha}+\bar{\beta}}{2}\,(1+z)^2+\frac{\bar{\alpha}-\bar{\beta}}{2}\,(1-z)^2\right]. \qquad (3)
\end{aligned}
$$

Here, and in the following, $z = \cos\theta_\gamma$. The differential cross-section of a point-like proton is given by

$$
\begin{aligned}
\left(\frac{{\rm d}\sigma}{{\rm d}\Omega}\right)_{\rm Point} &= \frac{1}{2}\left(\frac{e^2}{m}\right)^2\left(\frac{\omega'}{\omega}\right)^2\left\{1+z^2\right. \\
&\left.+\frac{\omega\omega'}{m^2}\left([1-z]^2+a_0+a_1 z+a_2 z^2\right)\right\}, \qquad (4)
\end{aligned}
$$

with the coefficients:

$$
\begin{aligned}
a_0 &= 2\kappa+\tfrac{9}{2}\kappa^2+3\kappa^3+\tfrac{3}{4}\kappa^4\,, \\
a_1 &= -4\kappa-5\kappa^2-2\kappa^3\,, \\
a_2 &= 2\kappa+\tfrac{1}{2}\kappa^2-\kappa^3-\tfrac{1}{4}\kappa^4\,.
\end{aligned}
$$

For $\kappa = 0$ one obtains the Klein-Nishina cross-section [7] for scattering from a point-like charged particle with spin $1/2$.

The low-energy expansion of the Compton scattering amplitude to the order $\omega\omega'$ can be used up to about 80 MeV incident photon energy to extract $\bar{\alpha}$ and $\bar{\beta}$ in an almost model-independent way from the measured differential cross-sections. With increasing energy the influence of higher-order terms has to be taken into account. The next-order terms are described by the four spin polarizabilities of the proton, γ_{E1}, γ_{M1}, γ_{E2} and γ_{M2} [8], two combinations of which are of special interest. These are the forward and backward spin polarizabilities:

$$
\gamma = -\gamma_{E1}-\gamma_{M1}-\gamma_{E2}-\gamma_{M2} \qquad (5)
$$

and

$$
\gamma_\pi = -\gamma_{E1}+\gamma_{M1}+\gamma_{E2}-\gamma_{M2}\,, \qquad (6)
$$

respectively [2]. Since the cross-sections are already dominated by the excitation of the Δ-resonance at these energies, it is expected that the magnetic spin polarizabilities are mainly given by the magnetic excitation of the Δ-resonance.

2 Compton scattering at higher energies

At photon energies close to π-production threshold and above, an expansion of the scattering amplitude in orders of the photon energy no longer makes sense and reliable model calculations do not exist. Therefore, the dispersion relation approach developed by L'vov [9] was used in the present work. In this formalism the ingredients of the calculation are partially fixed by experimental results, *i.e.* by the multipoles of meson photoproduction. Other mechanisms which dominate Compton scattering can therefore be investigated in great detail, *i.e.* t-channel exchanges of mesons coupling to two photons.

The scattering process is described by six invariant amplitudes A_i for which the real parts can be written at fixed t as [5,9]

$$
{\rm Re}A_i(\nu,t) = A_i^{\rm Born}(\nu,t)+A_i^{\rm int}(\nu,t)+A_i^{\rm as}(\nu,t). \qquad (7)
$$

The first term on the r.h.s. is the Born contribution. It corresponds to $({\rm d}\sigma/{\rm d}\Omega_{\rm Point})$ in eq. (3) and is completely determined by the proton's charge, mass and magnetic moment. The second term on the r.h.s of eq. (7), $A_i^{\rm int}(\nu,t)$, is an integral part where the dispersion integral is evaluated from pion production threshold $\nu_{\rm thr}$, with

[1] The polarizabilities $\bar{\alpha}$ and $\bar{\beta}$ are given in units of $10^{-4}\,{\rm fm}^3$ throughout this article.

[2] The spin polarizabilities γ and γ_π are given in units of $10^{-4}\,{\rm fm}^4$ throughout this article.

$\omega_{\rm thr} = \nu_{\rm thr}(t) - t/4m = 150$ MeV, to a maximum energy, $\nu_{\rm max}$, for which $\omega_{\rm max} = \nu_{\rm max}(t) - t/4m$ is taken to be equal to 1.5 GeV [9]:

$$A_i^{\rm int}(\nu,t) = \frac{2}{\pi}\mathcal{P}\int\limits_{\nu_{\rm thr}}^{\nu_{\rm max}} \frac{\nu' {\rm Im}A_i(\nu',t)}{\nu'^2-\nu^2}{\rm d}\nu' \,. \tag{8}$$

The third term in eq. (7), $A_i^{\rm as}(\nu,t)$, is the asymptotic part which contains all contributions to the amplitude from above $\nu_{\rm max}$.

The imaginary parts of the amplitudes A_i can be expressed via the optical theorem, *i.e.* by making use of the unitarity condition, mainly in terms of products of single π-photoproduction multipoles supplemented by two-pion contributions. A detailed description of all the ingredients can be found in ref. [9].

In this formalism it can be shown that the Baldin sum rule fixes the non-Born part of the amplitudes A_3 and A_6 in forward direction at $\nu = t = 0$:

$$\bar\alpha + \bar\beta = -\frac{1}{2\pi}\left[A_{3+6}^{\rm int}(0,0) + A_{3+6}^{\rm as}(0,0)\right] \tag{9}$$

$$= \frac{1}{2\pi^2}\int\limits_{\omega_{\rm thr}}^{\infty}\frac{\sigma_{\rm tot}(\omega')}{\omega'^2}{\rm d}\omega' \,. \tag{10}$$

It can also be deduced from the non-Born part of A_4 at $\nu = t = 0$ that

$$A_4^{\rm nB}(0,0) = \frac{m}{2\pi}\int\limits_{\nu_{\rm thr}}^{\infty}\frac{\sigma_{1/2} - \sigma_{3/2}}{\nu'^3}{\rm d}\nu' \,, \tag{11}$$

which is equivalent to the forward spin polarizability sum rule. In eq. (11) $\sigma_{1/2}$ and $\sigma_{3/2}$ are the absorption cross-sections for definite helicity states of the incident photon and proton. This is another constraint on the invariant amplitudes as far as A_4 is concerned:

$$\gamma = \frac{1}{2\pi m}\left[A_4^{\rm int}(0,0) + A_4^{\rm as}(0,0)\right] \,. \tag{12}$$

Additional constraints of the invariant amplitudes at $\nu = t = 0$ arise which are related to backward scattering:

$$\bar\alpha - \bar\beta = -\frac{1}{2\pi}A_1^{\rm nB}(0,0) \,, \tag{13}$$

$$\gamma_\pi = -\frac{1}{2\pi m}\left[A_2^{\rm nB}(0,0) + A_5^{\rm nB}(0,0)\right] \,. \tag{14}$$

The quantity γ_π in eq. (14) is the backward spin polarizability introduced in eq. (6).

The amplitudes $A_i(\nu,t)$ approach zero in the high-energy limit at fixed t [9] except for the two amplitudes $A_1(\nu,t)$ and $A_2(\nu,t)$ which are assumed to be proportional to $\nu^{\alpha(t)}$, where $\alpha(t) \leq 1$ is the Regge trajectory. Therefore, these latter two amplitudes require special consideration. In the case of the amplitude $A_1(\nu,t)$ the non-Born part taken at $\nu = t = 0$ is related to the difference $\bar\alpha - \bar\beta$ of the electromagnetic polarizabilities, whereas the non-Born part of the amplitude $A_2(\nu,t)$ is related to the backward spin polarizability γ_π. Note that neither of these latter amplitudes contributes to forward scattering. The integral parts are completely determined by the multipoles of π-photoproduction and the asymptotic contributions are related to the t-channel exchange of the lightest scalar and pseudo-scalar particles which are the σ- and π^0-meson. Since the "σ-meson" has never been observed directly, it is more suitable to assign it to a 2π-exchange.

Such t-channel exchanges are commonly described by a pole diagram located at the meson mass, which in case of a π^0-exchange is called the Low-amplitude [9]:

$$A_2^{\rm as}(\nu,t) \approx A_2^{\pi^0}(t) = \frac{g_{\pi NN}F_{\pi^0\gamma\gamma}}{t - m_{\pi^0}^2}F_\pi(t) \,. \tag{15}$$

The product of the πNN and $\pi^0\gamma\gamma$ coupling constants is taken to be $g_{\pi NN}F_{\pi^0\gamma\gamma} = (-0.333 \pm 0.012)$ GeV^{-1} [9]. The Low-amplitude is extended by an off-shell form factor

$$F_\pi(t) = \frac{\Lambda_\pi^2 - m_\pi^2}{\Lambda_\pi^2 - t} \tag{16}$$

with the cutoff parameter $\Lambda_\pi = 700$ MeV. The same may be applied to the σ-exchange in the t-channel:

$$A_1^{\rm as}(\nu,t) \approx \frac{g_{\sigma NN}F_{\sigma\gamma\gamma}}{t - m_\sigma^2} \,. \tag{17}$$

The absence of a form factor is motivated by the unknown mass of the "σ-meson" which serves as a parameter to reproduce the cross-sections at backward angles at photon energies above the Δ-resonance range. A good description of such data has been achieved with $m_\sigma = 600$ MeV [9, 10] which will be used for the present investigation.

2.1 Re-evaluation of the sum rules

The photon absorption cross-section of the proton (fig. 1) has been measured by Armstrong *et al.* [11] with tagged photons in the energy range from 265 MeV to 4215 MeV in the early 1970s. In fig. 1 the results are compared with the very precise data obtained recently in the energy range from 200 MeV to 800 MeV [12] at the tagged photon beam in Mainz [13,14]. In the Δ-resonance region there is a slight difference between both measurements. The absorption cross-section as obtained from the partial wave analysis by Arndt *et al.* [15], using the solution SAID-SM99K (shown as solid line in the insert of fig. 1), exhibits rather good agreement with the Mainz data in the Δ-resonance region.

To evaluate the Baldin sum rule, the absorption cross-section has been divided into the following energy intervals:

$$\begin{aligned} &\mathcal{I}_1 : \omega \in [145, 200) \,, \\ &\mathcal{I}_2 : \omega \in [200, 2000) \,, \\ &\mathcal{I}_3 : \omega \in [2000, \infty) \,. \end{aligned} \tag{18}$$

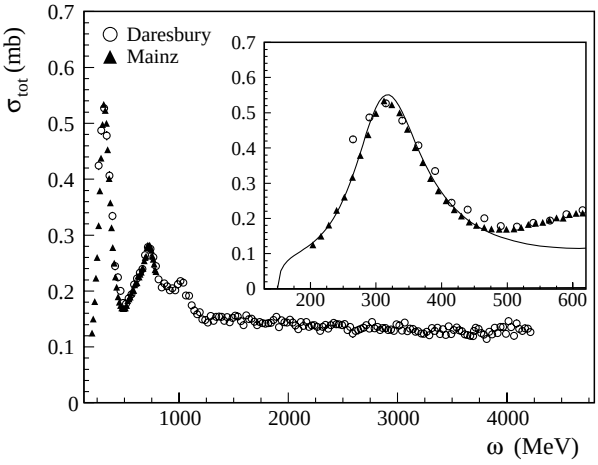

Fig. 1. The total photon absorption cross-section of the proton as measured by Armstrong *et al.* (Daresbury) [11] and McCormick *et al.* (Mainz) [12]. The insert shows the energy region up to 600 MeV magnified. The statistical errors of both experiments are within the symbol size. The prediction for single π-production as calculated from the partial wave analysis of Arndt *et al.* [15] solution SAID-SM99K (shown as solid line in the insert) shows that up to about 450 MeV the absorption cross-section is predominantly given by this process.

Table 1. Contributions to the Baldin sum rule in units of 10^{-4} fm^3. The different energy intervals are defined in eq. (18). For the low-energy interval $\mathcal{I}_1$ various solutions of the partial wave analysis by Arndt *et al.* [15] were used to calculate their contribution. For $\mathcal{I}_3$ the result of ref. [16] is given. The errors include the experimental errors of the data points, *i.e.* statistical and systematic errors, and an estimated error for the integration method due to the spacing between the data points.

Solution	$\mathcal{I}_1$(SAID)	$\mathcal{I}_2$(data)	$\mathcal{I}_3$ (ref. [16])
SM99K	1.39 ± 0.04	11.82 ± 0.36	0.73 ± 0.03
WI98K	1.19 ± 0.04	–	–
SP97K	1.19 ± 0.04	–	–
SM95	1.32 ± 0.04	–	–
Average	1.27 ± 0.10	11.82 ± 0.36	0.73 ± 0.03

In the interval $\mathcal{I}_1$ the cross-section obtained from the partial wave analysis will be used. The Mainz data cover the energy range from 200 MeV to 800 MeV, and at energies above, the Armstrong data complete the cross-sections in the interval $\mathcal{I}_2$. Above 2000 MeV the method of ref. [16] which uses an overall function fitted to the measured cross-sections, has been adopted. In table 1 the results of the re-evaluation of the Baldin sum rule are tabulated [3]. The low-energy interval $\mathcal{I}_1$ contributes about 10% to the sum rule value and is strongly dependent on the partial wave analysis used. In order to take such a "theoretical" uncertainty properly into account, we use the average for $\mathcal{I}_1$, *i.e.* 1.3 ± 0.1, and the standard deviation of the tabulated values as the error. The Baldin sum rule is then evaluated to be

$$\bar{\alpha} + \bar{\beta} = (13.8 \pm 0.4) \ . \tag{19}$$

This result is, of course, in agreement with that of ref. [16], which is (13.69 ± 0.14), since the same cross-section data were used. The difference reflects i) the contribution of the energy region close to π-threshold, *i.e.* interval $\mathcal{I}_1$, and ii) that in ref. [16] the data points were fitted to obtain an excellent representative function for the integration.

Sometimes the values (14.2 ± 0.3) [17] or (14.2 ± 0.5) [18] are quoted. The first had been obtained from an analysis of the absorption cross-sections measured in the late 1960s at SLAC and DESY. These experiments have partially been published by Caldwell *et al.* [19] and Ballam *et al.* [20]. The second value is based on the partial wave analysis of Pfeil *et al.* [21] and Moorhouse *et al.* [22]. In the following the new value of the Baldin sum rule, eq. (19), will be used.

[3] The trapezoidal rule integration provided by the CERNlib has been used to evaluate the integrals.

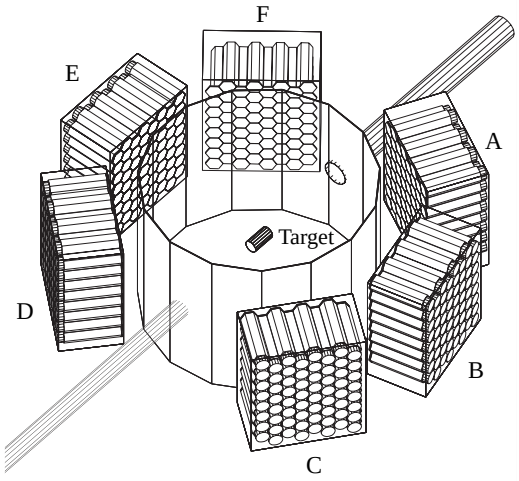

Fig. 2. The TAPS detector at MAMI. The photon beam enters the setup between the blocks A and F. Also shown are target cell and scattering chamber.

3 Experiment

Low-energy Compton scattering from the proton [23] in the energy range from 55 MeV to 165 MeV was measured using the TAPS detector system [24] (fig. 2) set up at the photon beam [13] at MAMI [14]. The energy of the incident electron beam was chosen to be 180 MeV. The emitted bremsstrahlung beam was collimated resulting in a tagging efficiency of about 17% (measured at low intensity with a BGO detector in the direct photon beam). This low tagging efficiency has its origin in the low incident electron energy and the collimation system behind the tagger.

The target consisted of a Kapton cylinder of 20 cm length filled with liquid hydrogen. The target thickness

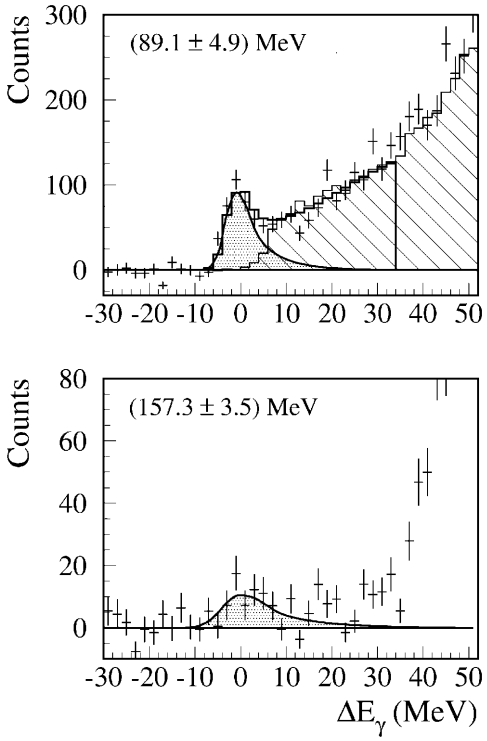

Fig. 3. Missing-energy spectra at $\theta_\gamma = 59°$ (+). The shaded area corresponds to the simulated response to elastically scattered photons. Top: spectrum below the π-production threshold. The hatched area is the measured spectrum of charged particles adjusted to the photon missing-energy spectrum. Bottom: spectrum above the π-production threshold. The rise in intensity at larger missing energy is due to π^0-production.

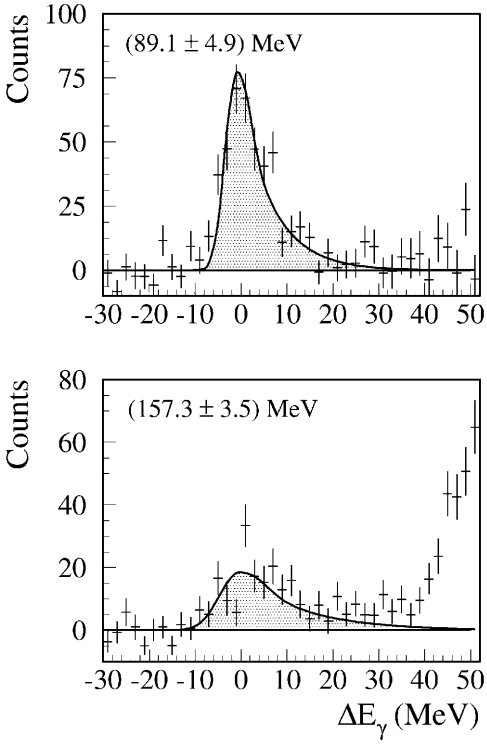

Fig. 4. Same as fig. 3 for $\theta_\gamma = 133°$.

was $N_{\mathrm{T}} = (8.66 \pm 0.18) \cdot 10^{23}$ cm^{-2}. Data obtained from about 200 h of beam time were analyzed.

The scattered photons were detected with the 6 blocks A to F of the TAPS detector (fig. 2). Since the recoiling protons could not be detected, a single-particle trigger had to be used, *i.e.* the minimum block multiplicity was set to 1 in order to create the trigger signal. Therefore, this minimum bias trigger included all kinds of background events. There are cosmic ray events which have not been suppressed by an active shield. There is electromagnetic background from the beam collimation system and from the target itself which hits the blocks installed close to the beam. These sources of background were partially suppressed by restrictive time cuts.

The missing-energy ΔE_γ which is defined as the difference between the measured incident photon energy (as given by the tagger) and the expected incident photon energy (as calculated from the measured momentum of the scattered photon assuming Compton kinematics), $\Delta E_\gamma = \omega - E_\omega^{\mathrm{TAPS}}$, allows a combination of several tagging channels in one spectrum without losing the energy resolution by binning over tagger channels. Such spectra are shown in figs. 3 and 4 for $\theta_\gamma = 59°$ and 133° at incident photon energies of 89.1 MeV and 157.3 MeV. The peak of elastically scattered photons appears at zero missing energy. At forward angles and low photon energies (upper spectrum in fig. 3) the background produced in the target mainly originates from pair production. Such events are only partially suppressed by the veto detectors. Therefore, by identifying these charged particles with the veto detectors, the missing-energy distributions of these events could be measured and then normalized to the measured photon missing-energy distribution above 20 MeV (hatched area in fig. 3).

Above the π-production threshold (lower spectra in figs. 3 and 4) additional photons arise due to π^0-photoproduction followed by their immediate 2γ-decay. These events are clearly separated from the elastically scattered photons. Thus, the number of scattered photons could be extracted using the simulated response of TAPS to scattered photons.

4 Electromagnetic polarizabilities $\bar{\alpha}$ and $\bar{\beta}$

The differential cross-sections obtained are tabulated in table 2 and plotted in comparison with previous experiments in fig. 5. The systematic (normalization) errors of ±3%, which affect all measured cross-sections in common, arise from uncertainties in the photon flux (±2%) and target density (±2%) combined in quadrature. The effective solid angles were determined with Monte Carlo simulations. Errors from uncertainties in the experiment geometry and from the statistics of the simulation may be treated as individual (random) errors (random systematic errors). They are estimated to be ±5%. During the fitting procedure, as explained below, this error has

Table 2. The measured differential cross-sections (lab system). The errors given are statistical only.

ω (MeV)	$\theta_\gamma = 59°$	$\theta_\gamma = 85°$	$\theta_\gamma = 107°$
58.94	13.20 ± 0.65	11.44 ± 0.60	12.43 ± 0.62
69.05	13.70 ± 0.69	10.70 ± 0.60	12.98 ± 0.68
79.19	12.95 ± 0.71	9.92 ± 0.60	13.70 ± 0.72
89.11	11.24 ± 0.70	10.97 ± 0.68	11.74 ± 0.70
98.90	10.53 ± 0.77	10.79 ± 0.74	11.61 ± 0.73
108.42	9.19 ± 0.72	10.76 ± 0.80	12.15 ± 0.79
117.60	11.63 ± 0.91	12.51 ± 0.92	11.62 ± 0.80
126.40	7.88 ± 0.83	10.06 ± 0.92	15.39 ± 1.11
134.73	9.72 ± 1.00	11.03 ± 1.04	14.32 ± 1.10
142.58	9.30 ± 1.06	11.46 ± 1.25	15.33 ± 1.16
149.87	9.90 ± 1.22	14.07 ± 1.42	15.90 ± 1.39
157.31	9.08 ± 1.35	17.05 ± 1.77	20.08 ± 1.73
163.71	11.60 ± 1.47	18.17 ± 1.92	21.36 ± 1.91
ω (MeV)	$\theta_\gamma = 133°$	$\theta_\gamma = 155°$	
58.94	14.19 ± 0.71	19.03 ± 0.91	
69.05	13.71 ± 0.71	17.64 ± 0.88	
79.19	13.11 ± 0.72	18.27 ± 0.91	
89.11	12.91 ± 0.74	20.60 ± 1.02	
98.90	14.06 ± 0.84	18.02 ± 0.97	
108.42	10.84 ± 0.77	17.52 ± 1.03	
117.60	14.58 ± 0.99	20.39 ± 1.27	
126.40	16.14 ± 1.12	16.71 ± 1.12	
134.73	15.15 ± 1.11	19.33 ± 1.30	
142.58	18.87 ± 1.43	19.67 ± 1.34	
149.87	19.14 ± 1.62	22.61 ± 1.68	
157.31	21.80 ± 1.86	30.55 ± 2.10	
163.71	25.13 ± 2.10	32.01 ± 2.31	

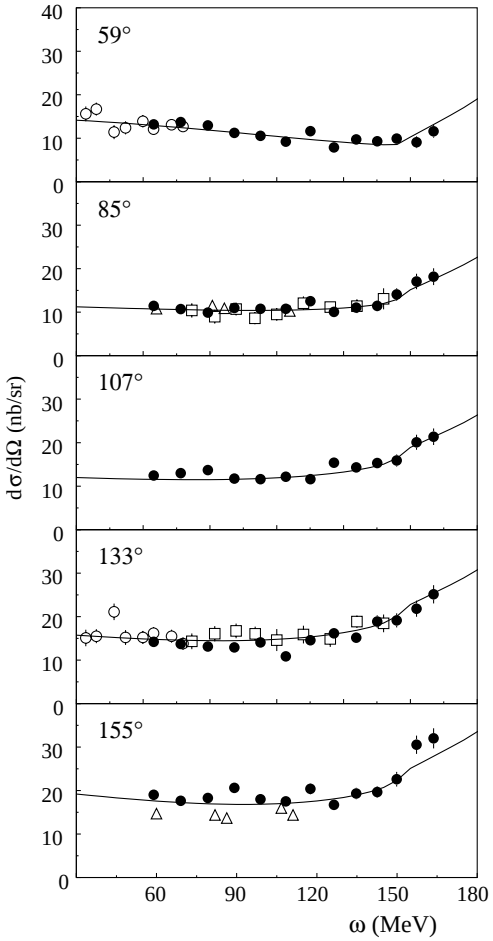

Fig. 5. The measured differential cross-sections in the lab system as obtained by the TAPS experiment (•) [23]. The additional data are taken from ref. [26] (○), ref. [27] (□) and ref. [25] (△). The statistical errors are partially within the symbol size. The solid line shows the calculation of the dispersion relation approach using the π-production multipoles of Arndt *et al.* [15], solution SAID-SM99K. The polarizabilities were chosen to be: $\bar{\alpha} + \bar{\beta} = 13.8$, $\bar{\alpha} - \bar{\beta} = 10.5$ and $\gamma_\pi = -37.1$.

therefore been added in quadrature to the statistical errors of the individual data points. The latter are given in table 2.

The overall agreement between the different experiments is very satisfactory, except for the 150° data of ref. [25]. The calculations within the dispersion relation approach using the π-photoproduction multipoles of Arndt *et al.* [15], solution SAID-SM99K, and best-fit values for the polarizabilities (see below) are included in the figure as solid lines.

With the help of the dispersion relation approach the electromagnetic polarizabilities of the proton can be extracted from the experimental cross-sections. Due to the constraints of the invariant scattering amplitudes the difference $\bar{\alpha} - \bar{\beta}$ and the sum $\bar{\alpha} + \bar{\beta}$ may be used as free parameters or equivalently $\bar{\alpha}$ and $\bar{\beta}$. The procedure used in this work was to take $\bar{\alpha}$ and $\bar{\beta}$ as free parameters, and sometimes as well the constraint given by the Baldin sum rule as a single datum. Using standard χ^2 minimization [4], the result obtained, when fitting the TAPS data alone without the sum rule constraint, is

$$\begin{aligned} \bar{\alpha} &= 11.9 \pm 0.5(\text{stat.}) \mp 1.3(\text{syst.}) \,, \\ \bar{\beta} &= 1.2 \pm 0.7(\text{stat.}) \pm 0.3(\text{syst.}) \,, \end{aligned} \tag{20}$$

with $\chi^2_{\text{red}} = {}^{80.8}/_{65\text{-}2} = 1.28$. The errors given are the statistical (including the "random systematic" error) and systematic error. The Baldin sum rule obtained from this result, $\bar{\alpha} + \bar{\beta} = 13.1 \pm 0.9 \mp 1.0$, is in agreement with the value given in eq. (19), within the errors. The systematic errors in eq. (20) were obtained by re-scaling the differential cross-sections by $\pm 3\%$ according to the common normalization error. The low-energy data of Federspiel *et al.* [26], MacGibbon *et al.* [27] and Zieger *et al.* [28] were treated in the same way which resulted in the polarizabilities in table 3.

When fitting independent experiments the procedure above is not suitable. A different way of using systematic errors in fitting procedures was proposed in ref. [29]. There it is assumed that the systematic error is an energy-independent normalization error which can be treated like a statistical one. Therefore, according to ref. [29],

[4] For the fitting procedure the program package MINUIT from the CERNlib was used.

Table 3. The polarizabilities $\bar{\alpha}$ and $\bar{\beta}$ as obtained by fitting the differential cross-sections from different experiments. The errors given are the statistical and systematic ones. *fixed* denotes that $\bar{\alpha}+\bar{\beta}=13.8\pm0.4$ was included as a single datum. The data of Zieger have been fitted with $\bar{\alpha}-\bar{\beta}$ as the only parameter. The last line shows the result of the global fit for which all data sets were allowed to vary according to their systematic errors.

Data		$\bar{\alpha}+\bar{\beta}$ *fixed*	$\bar{\alpha}+\bar{\beta}$ *free*
TAPS	$\bar{\alpha}$	$12.1\pm0.4\mp1.0$	$11.9\pm0.5\mp1.3$
(this work)	$\bar{\beta}$	$1.6\pm0.4\pm0.8$	$1.2\pm0.7\pm0.3$
MacGibbon	$\bar{\alpha}$	$11.9\pm0.5\mp0.8$	$12.6\pm1.2\mp1.3$
[27]	$\bar{\beta}$	$1.9\pm0.5\pm0.8$	$3.0\pm1.8\pm0.1$
Federspiel	$\bar{\alpha}$	$10.8\pm2.2\mp1.3$	$10.1\pm2.6\mp2.0$
[26]	$\bar{\beta}$	$3.0\pm2.2\pm1.3$	$2.0\pm3.3\pm0.3$
Zieger	$\bar{\alpha}-\bar{\beta}$	$6.4\pm2.3\pm1.9$	
[28]			
Global	$\bar{\alpha}$	$12.1\pm0.3\mp0.4$	$11.9\pm0.5\mp0.5$
Fit	$\bar{\beta}$	$1.6\pm0.4\pm0.4$	$1.5\pm0.6\pm0.2$

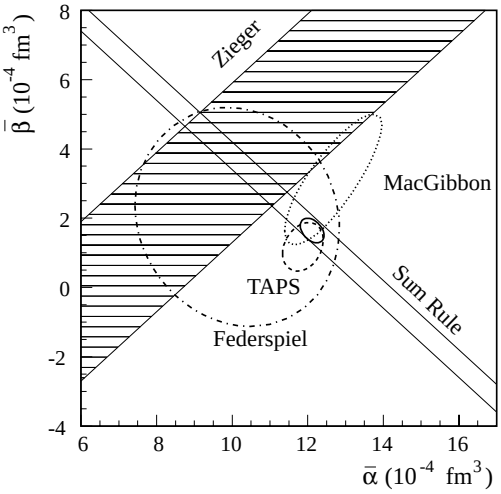

Fig. 6. Error contour plot in the ($\bar{\alpha}$-$\bar{\beta}$)-plane of the experiments in table 3 (last column) for which the errors are taken as the statistical ones only. The contours correspond to the values $\chi^2_{\rm min}+1$ of the individual fits. Also shown are the sum rule constraint and the value $\bar{\alpha}-\bar{\beta}$ as follows from the experiment by Zieger *et al.* [28]. The thick solid line shows the result of the global fit, eq. (22).

an extended χ^2-function,

$$\chi^2=\sum\left[\left(\frac{N\sigma_{\rm exp}-\sigma_{\rm theo}}{N\Delta\sigma}\right)^2\right]+\left(\frac{N-1}{\Delta\sigma_{\rm sys}}\right)^2\ , \quad (21)$$

can be minimized. Here N is a normalization parameter used to change the normalization for each data set within its systematic errors $\Delta\sigma_{\rm sys}$. A fit to the low-energy data of refs. [26–28] and the new TAPS data, and the sum rule constraint of eq. (19) then leads to the following result ($\chi^2_{\rm red}={}^{108.6}/_{102\text{-}6}=1.13$):

$$\begin{aligned}\bar{\alpha}&=12.1\pm0.3(\text{stat.})\mp0.4(\text{syst.})\pm0.3(\text{mod.})\ ,\\ \bar{\beta}&=\ \ 1.6\pm0.4(\text{stat.})\pm0.4(\text{syst.})\pm0.4(\text{mod.})\ ,\end{aligned} \quad (22)$$

where the first error denotes the statistical, the second the systematic and the third the model-dependent one. The results of table 3 can be summarized as in fig. 6 where the contours in the ($\bar{\alpha}$-$\bar{\beta}$)-plane for $\chi^2_{\rm min}+1$ are plotted. In addition, the Baldin sum rule and the value obtained from the experiment by Zieger *et al.* [28] are included. The thick solid line then is the result of eq. (22) with the statistical error only.

The model-dependent errors in eq. (22) have been estimated by varying the main parameters entering the calculation. These are:

- the coupling constants $g_{\pi NN}F_{\pi^0\gamma\gamma}$:
  $\Delta g_{\pi NN}F_{\pi^0\gamma\gamma}=\pm3.6\%\Rightarrow\Delta\bar{\alpha}(\bar{\beta})\approx\mp0.13(\pm0.13)$;
- the cutoff parameter Λ_π of the π^0-form factor:
  $\Delta\Lambda_\pi=\pm100$ MeV $\Rightarrow\Delta\bar{\alpha}(\bar{\beta})\approx\mp0.12(\pm0.12)$;
- the strength of the M_{1+} multipole:
  $\Delta M_{1+}=\pm1\%\Rightarrow\Delta\bar{\alpha}(\bar{\beta})\approx\pm0.10(\mp0.10)$;
- the $\frac{E2}{M1}$ ratio of the resonance multipoles:
  $\Delta\frac{E2}{M1}=\pm1\%\Rightarrow\Delta\bar{\alpha}(\bar{\beta})\approx\mp0.08(\pm0.08)$;
- the σ-mass parameter m_σ:
  $\Delta m_\sigma=\pm20$ MeV $\Rightarrow\Delta\bar{\alpha}(\bar{\beta})\approx\mp0.04(\pm0.05)$;
- the backward spin polarizability γ_π:
  $\Delta\gamma_\pi=\pm1\Rightarrow\Delta\bar{\alpha}(\bar{\beta})\approx\pm0.26(\mp0.26)$.

These contributions were obtained by keeping the normalization factors fixed. The total model-dependent errors were then taken as the individual contributions added in quadrature. Since $\Lambda_\pi=700$ MeV is "*estimated from the axial radius of the nucleon and the size of the pion*" (see ref. [9] and references therein), the uncertainties of these quantities can be used to estimate an uncertainty of $\Delta\Lambda_\pi=\pm100$ MeV. Another error estimate, *i.e.* $\Delta m_\sigma=\pm20$ MeV, is based on new experimental data on Compton scattering from the proton above the Δ-resonance [10]. For these new data a good description has been achieved for $m_\sigma=600$ MeV within a range of about ±20 MeV.

From eq. (22) it follows that the difference of the electromagnetic polarizabilities is

$$\bar{\alpha}-\bar{\beta}=10.5\pm0.9(\text{stat.}+\text{syst.})\pm0.7(\text{mod.})\ . \quad (23)$$

This will be taken as the new global average. A comparison with the global average as evaluated by MacGibbon *et al.* [27], $\bar{\alpha}-\bar{\beta}=10.0\pm1.5\pm0.9$, exhibits the improvement achieved with the TAPS experiment. The experimental error has been reduced by almost a factor $^2/_3$. Agreement has also been achieved with the LEGS group. Their results [30]

$$\bar{\alpha}+\bar{\beta}=13.23\pm0.86(\text{stat.}+\text{syst.})\ , \quad (24)$$

$$\bar{\alpha}-\bar{\beta}=10.11\pm1.74(\text{stat.}+\text{syst.})\ , \quad (25)$$

are consistent with ours, as far as $\bar{\alpha}$ and $\bar{\beta}$ are concerned.

5 Backward spin polarizability γ_π

The above results were obtained using a fixed value of the backward spin polarizability $\gamma_\pi = -37.1$. The wide angular and energy range of the TAPS experiment also allows investigation of γ_π in more detail.

The backward spin polarizability γ_π is given by the non-Born contributions of the invariant amplitudes A_2 and A_5. Only the asymptotic part of A_2 is left as a source for an additional contribution beyond the π^0-exchange in the t-channel. In this analysis such a contribution has been modeled with a t-dependent term in the form of a monopole form factor,

$$A_2^{\rm as}(\nu,t) \approx A_2^{\pi^0}(t) - 2\pi m \frac{\delta\gamma_\pi}{1-\frac{t}{\Lambda^2}} \ , \qquad (26)$$

from which the substitution follows:

$$\gamma_\pi \rightarrow \gamma_\pi + \delta\gamma_\pi \ . \qquad (27)$$

The parameter Λ defines the slope of the function at $t = 0$ and is chosen to be $\Lambda = 700$ MeV. In varying $\delta\gamma_\pi$ the influence of any deviation from the standard value of γ_π can be investigated in terms of this ansatz.

Using the same fitting procedure as described above, the result as obtained from the TAPS data alone without the sum rule constraint is

$$\begin{aligned} \bar{\alpha} &= \ \ 12.2 \pm 0.8(\text{stat.}) \mp 1.4(\text{syst.}) \ , \\ \bar{\beta} &= \ \ \ 0.8 \pm 0.9(\text{stat.}) \pm 0.5(\text{syst.}) \ , \\ \gamma_\pi &= -35.9 \pm 2.3(\text{stat.}) \mp 0.4(\text{syst.}) \ , \end{aligned} \qquad (28)$$

with $\chi^2_{\rm red} = {}^{80.6}/_{65\text{-}3} = 1.30$. A fit to all low-energy data including the sum rule constraint yields

$$\begin{aligned} \bar{\alpha} &= \ \ 12.4 \pm 0.6(\text{stat.}) \mp 0.5(\text{syst.}) \pm 0.1(\text{mod.}) \ , \\ \bar{\beta} &= \ \ \ 1.4 \pm 0.7(\text{stat.}) \pm 0.4(\text{syst.}) \pm 0.1(\text{mod.}) \ , \\ \gamma_\pi &= -36.1 \pm 2.1(\text{stat.}) \mp 0.4(\text{syst.}) \pm 0.8(\text{mod.}) \ , \end{aligned} \qquad (29)$$

with $\chi^2_{\rm red} = {}^{108.4}/_{102\text{-}7} = 1.14$. From these results one obtains the difference of the electromagnetic polarizabilities

$$\bar{\alpha} - \bar{\beta} = 11.0 \pm 1.3(\text{stat.+syst}) \pm 0.1(\text{mod.}) \ . \qquad (30)$$

Compared to the result of eq. (23) the larger statistical and systematic error is compensated by the reduced model-dependent error. The latter effect is absorbed into the large error of γ_π in eq. (29).

The extracted value of γ_π, eq. (29), is in accordance with our findings in Compton scattering above 200 MeV [31,10]. There is no indication of any modification of the asymptotic contribution $A_2^{\rm as}$. This statement is confirmed by the LARA experiment [10] from which

$$\gamma_\pi = -37.9 \pm 0.6(\text{stat.} + \text{syst.}) \pm 3.5(\text{mod.}) \qquad (31)$$

had been extracted. Looking at γ_π, the difference between the LARA and TAPS experiment can be seen in the different size of the errors. Whereas our low-energy TAPS results give a rather large experimental error of ± 2.3, the model-dependent error of ± 3.5 dominates the "high-energy" LARA experiment. This exhibits the fact that the influence of γ_π increases with increasing photon energy.

Despite the good agreement of the electromagnetic polarizabilities between the results presented here and the ones published by the LEGS group [30], see eqs. (24) and (25), our value of γ_π contradicts the LEGS value [30] which is

$$\gamma_\pi = -27.1 \pm 2.2(\text{stat.} + \text{syst.}) \pm 2.6(\text{mod.}) \ . \qquad (32)$$

As already described in ref. [10], this contradiction has its main origin in the disagreement of the measured cross-sections above the π-threshold mainly at backward angles.

6 Summary

Differential cross-sections for Compton scattering at photon energies from 55 MeV to 165 MeV have been measured at five scattering angles between 59° and 155°. The electromagnetic polarizabilities of the proton have been extracted using dispersion relations. The new global average $\bar{\alpha} - \bar{\beta} = 10.5 \pm 0.9(\text{stat.} + \text{syst.}) \pm 0.7(\text{mod.})$ confirms the old global average of MacGibbon *et al.* [27] with a reduced experimental error. This new global average includes the Baldin sum rule $\bar{\alpha} + \bar{\beta} = 13.8 \pm 0.4$ which has been re-evaluated from the measured absorption cross-sections.

The extracted value of the backward spin polarizability $\gamma_\pi = -36.1 \pm 2.1(\text{stat.} + \text{syst.}) \pm 0.8(\text{mod.})$ is in agreement with our results above 200 MeV [31,10]. The conclusion to be drawn is that the obtained differential cross-sections do not show any indication of an additional asymptotic contribution to the amplitude A_2. Such a contribution, as suggested by the LEGS group [30], would modify the value of γ_π considerably.

We would like to express our gratitude to the MAMI staff for delivering always a perfect beam and for their technical support. We thank A.I. L'vov for supplying us with his code. F.W. wants to thank B. Muhl and H. Daam, Mainz, for their hospitality during the experiments. This work was supported by Deutsche Forschungsgemeinschaft (SFB 201).

References

1. F.E. Low, Phys. Rev. **96**, 1428 (1954).
2. M. Gell-Mann, H.Z. Goldberger, Phys. Rev. **96**, 1433 (1954).
3. A. Klein, Phys. Rev. **99**, 998 (1955).
4. V.A. Petrun'kin, Sov. Phys. JETP **13**, 808 (1961).
5. V.A. Petrun'kin, Sov. J. Part. Nucl. **12**, 278 (1981).
6. J.L. Powell, Phys. Rev. **75**, 32 (1949).
7. O. Klein, Y. Nishina, Z. Phys. **52**, 853 (1929).
8. D. Babusci et al., Phys. Rev. C **58**, 1013 (1998).
9. A.I. L'vov, V.A. Petrun'kin, M. Schumacher, Phys. Rev. C **55**, 359 (1997).
10. G. Galler et al., Phys. Lett. B (in press).

11. T.A. Armstrong et al., Phys. Rev. D **5**, 1640 (1972).
12. M. MacCormick et al., Phys. Rev. C **53**, 41 (1996).
13. I. Anthony et al., Nucl. Instrum. Methods A **301**, 230 (1991); S.J. Hall et al., Nucl. Instrum. Methods A **368**, 698 (1996).
14. Th. Walcher, Prog. Part. Nucl. Phys. **24**, 189 (1990).
15. R.A. Arndt et al., Phys. Rev. C **53**, 430 (1996); The solution can be viewed using the program SAID via a TELNET call to `clsaid.phys.vt.edu` with user:said.
16. D. Babusci, G. Giordano, G. Matone, Phys. Rev. C **57**, 291 (1998).
17. M. Damashek, F.J. Gilman, Phys. Rev. D **1**, 1319 (1970).
18. A.I. L'vov, V.A. Petrun'kin, S.A. Startsev, Sov. J. Nucl. Phys. **29**, 651 (1979).
19. D.O. Caldwell et al., Phys. Rev. Lett. **23**, 1256 (1969).
20. J. Ballam et al., Phys. Rev. Lett. **21**, 1544 (1968). J. Ballam et al., Phys. Rev. Lett. **23**, 498 (1969).
21. W. Pfeil, D. Schwela, Nucl. Phys. B **45**, 379 (1972).
22. R.G. Moorhouse, H. Oberlack, A.H. Rosenfeld, Phys. Rev. D **9**, 1 (1974).
23. V. Olmos de León, Dissertation, Universität Mainz (2000).
24. R. Novotny, IEEE Trans. Nucl. Sci. **38**, 379 (1991).
25. P.S. Baranov et al., Phys. Lett. B **52**, 22 (1974); P.S. Baranov et al., Sov. J. Nucl. Phys. **21**, 355 (1975).
26. F.J. Federspiel et al., Phys. Rev. Lett. **67**, 1511 (1991).
27. B.E. MacGibbon et al., Phys. Rev. C **52**, 2097 (1995).
28. A. Zieger et al., Phys. Lett. B **278**, 34 (1992).
29. G. D'Agostini, Nucl. Instrum. Methods A **346**, 306 (1994).
30. J. Tonnison et al., Phys. Rev. Lett. **80**, 4382 (1998).
31. F. Wissmann et al., Nucl. Phys. A **660**, 232 (1999).